Sex-dependent plasticity of adult neural tissue in response to damage

Marina Recatalà-Martinez[1], Manel Bosch[2], Pedro Gaspar[3], Alessandro Mineo[3], Santiago Rios[1], Irene Miguel-Aliaga[3], Marta Morey[1,4,*]

1.Departament de Genètica, Microbiologia i Estadística, Facultat de Biologia, Universitat de Barcelona, Barcelona, Spain

2. Unitat de Microscòpia Òptica Avançada, Centres Científics i Tecnològics de la Universitat de Barcelona (CCiTUB), Barcelona, Spain

3. The Francis Crick Institute, London, United Kingdom.

4. Human Genetics and Disease, Institut de Biomedicina de la Universitat de Barcelona (IBUB), Barcelona, Spain

*Corresponding author: mmorey@ub.edu

KEY WORDS

neural tissue, adult plasticity, sex differences

ABSTRACT

Plasticity of intact adult neural tissue in the vicinity of neural damage serves to restore functionality of circuits. Much remains to be learned about the mechanisms regulating this process and the reported sex differences in recovery outcomes. Here, we present the fly gut and its innervation as a simplified model to address these questions. We show that gut damage caused by ingestion of toxic agents resulted in plasticity of the adult enteric neuronal network, manifested as a Reactive Oxygen Species (ROS)-dependent increase in neural tissue, which was reversible after a recovery period. Interestingly, males did not display neural plasticity, and masculinization of neurons in females suppressed the damage-dependent neural growth. Together, these findings position the fly gut as a system to investigate the cellular, molecular, and sex-specific underpinnings of neural plasticity, with implications for therapeutic advancements in neural circuit recovery.

SUMMARY STATEMENT

This study establishes the fly gut as a simple system to explore how adult neural tissues differ between sexes in their capacity for plasticity.

INTRODUCTION

Neural plasticity involves two key mechanisms for recovery after injury: axonal regeneration and structural plasticity of intact neural tissue. While axonal regeneration has been widely studied (Mahar and Cavalli, 2018; Tedeschi and Bradke, 2017), modulating the plasticity of remaining healthy neural tissue offers an alternative route to restore function (Gao et al., 2022; Petersen et al., 2022). Clinical evidence shows that this form of plasticity supports functional recovery and circuit reorganization after acute damage such as stroke (Cirillo et al., 2020; Murphy and Corbett, 2009; Nudo, 2003; Sampaio-Baptista et al., 2018) or multiple sclerosis episodes (Ksiazek-Winiarek et al., 2015; Prosperini et al., 2015). Notably, recovery outcomes show sex-specific differences (Turtzo and McCullough, 2008; Yu et al., 2015), suggesting variability in plasticity capacity (Hyer et al., 2018; Kirby et al., 2024).

Despite these observations, the molecular mechanisms regulating plasticity in intact adult neural tissue remain poorly understood. This is partly due to the technical challenges of studying healthy and damaged neurons in close proximity, which make it difficult to isolate and study specific structural plasticity processes. To address this, we developed a model that focuses on how intact neurons respond to non-neural tissue damage, using peripheral innervation as an accessible system. This allows for controlled injury and analysis of plasticity in a physiologically relevant yet simplified context.

We used the digestive tract of *Drosophila melanogaster* as a model system. Like in mammals, the fly gut is structurally and functionally compartmentalized (Buchon et al., 2013; Lemaitre and Miguel-Aliaga, 2013; Marianes and Spradling, 2013). Its epithelium includes intestinal stem cells (ISCs), enteroblasts (EBs), absorptive enterocytes (ECs), and secretory enteroendocrine (EE) cells. The gut is wrapped in muscle, oxygenated by a tracheal system, and innervated by neurons located in the central nervous system, the corpora cardiaca (neurosecretory structure), and the hypocerebral ganglion (HCG, one of the stomatogastric ganglia) (Kuraishi et al., 2015; Miguel-Aliaga et al., 2018). While most neurites target visceral muscle, some extend

to the underlying epithelium (Cognigni et al., 2011; Cui et al., 2024; Kenmoku et al., 2016; Petsakou et al., 2023). Unlike mammals, innervation in the fly gut is regionally restricted, making it well-suited for targeted analysis (Kuraishi et al., 2015; Miguel-Aliaga et al., 2018). Recent studies reveal that gastrointestinal neurons respond to factors such as microbiota, nutrients, aging, and reproductive state in flies and mammals (Ameku et al., 2020; Hadjieconomou et al., 2020). While functional plasticity has been observed in the posterior fly midgut during recovery (Petsakou et al., 2023), the mechanisms of structural plasticity in response to gut damage—and how they are shaped by biological sex—remain unexplored. Here, we show that intact neurons innervating the anterior midgut exhibit a female-specific, ROS-dependent, reversible structural plasticity, which is absent in male flies and suppressed in females with masculinized neurons.

RESULTS AND DISCUSSION

Intestinal damage induces reversible neural plasticity.

In order to quantify and characterize the innervation in the anterior part of the midgut, we proceeded to select a neural driver and reporter that would specifically label neuronal processes with native GFP fluorescence. This prevented background signal from secondary antibodies and provided a high signal-to-noise ratio, which facilitated faithful neural process quantification as GFP signal. General neuronal markers, such as Elav (Chen et al., 2016; Holsopple et al., 2022; Titos et al., 2023) or n-Synaptobrevin (Weaver et al., 2020), also label EEs. However, we used the *GMR51F12-GAL4* driver line from the Janelia FlyLight collection (Jenett et al., 2012; Min et al., 2021; Olds and Xu, 2014) and a specific *nSyb.S-GAL4* driver (Weaver et al., 2020), neither of which labels EEs. Morphological landmarks in whole-mount preparations, combined with phalloidin co-staining to visualize the surrounding musculature, enabled consistent imaging of the same digestive tract region and its associated neural innervation (Fig. 1A). Using 3D reconstruction and image analysis, we obtained volume quantifications for both the digestive tube and neural tissue (see Materials and Methods). Scaling growth is a prevalent phenomenon in the peripheral nervous system, where sensory and motor neurons must adjust the size of their arborizations according to the area of their target tissues to maintain their functionality (Bentley and Toroian-Raymond, 1981; Bucher and Pflüger, 2000; Lee and Stevens, 2007; Menon et al., 2013). Measuring the volume of the digestive tube enabled us to

use statistical analysis methods that accounted for and removed any potential influence of digestive tube size variation in adults (driven by treatment or genetic background) on neural tissue quantification comparisons and distinguish scaling growth from neural plasticity tissue growth (see Materials and Methods).

To damage the gut, we fed flies with DSS. DSS is a polymer that induces colitis in mammals (Yang and Merlin, 2024) and has been used in *Drosophila* to study the cellular mechanisms and molecular pathways that regulate ISC proliferation during regeneration (Jiang et al., 2016; Tian et al., 2022). When flies ingest DSS, it crosses the epithelium, expanding the basement membrane sheet and altering muscle morphology (Howard et al., 2019). The resulting change in biomechanical forces in the niche is thought to activate ISC division (Howard et al., 2019). DSS feeding also results in trachea sprouting (Perochon et al., 2021), which is necessary for ISC proliferation (Medina et al., 2025; Perochon et al., 2021; Tamamouna et al., 2021). Interestingly, basement membrane and muscle defects, as well as trachea remodeling, are reversible after a recovery period (Howard et al., 2019; Perochon et al., 2021; Tamamouna et al., 2021). We wondered whether adult neurons were plastic and could also respond to gut damage.

To analyze the effect of gut damage on neural plasticity, we fed adult mated females DSS for 4 days and compared them to controls fed with the carrier (sucrose) (Fig. S1A-D). We confirmed the effectiveness of DSS by replicating previously published observations, including a reduction in lifespan (Amcheslavsky et al., 2009) (data not shown), and an increase in the proliferative response of ISCs in the midgut (Amcheslavsky et al., 2009) (see later in Fig. 2A). Over 90% of the flies that survived the feeding protocol tested negative for the SMURF assay (Rera et al., 2012), indicating that in the majority of animals (93,3%±SD4.5) that were dissected gut permeability and integrity were not compromised (Fig. S1E,F). Thus, during DSS feeding, neurons were largely shielded from direct exposure to gut contents that could potentially cause them damage. When we dissected the DSS-fed females and compared them to control flies, we observed a significant increase in neural tissue (Fig. 1B). Virgin flies also showed a DSS-dependent increase in neural tissue, comparable in magnitude to that observed in mated females (Fig. S1H,I). To rule out

135 neurogenesis as the source of the new neural tissue, we quantified the number of
136 neural nuclei in the HCG, the primary source of neurons innervating the anterior
137 midgut (Fig. 1A). No differences were observed between control and DSS-fed animals
138 (Fig. 1C), suggesting that the increase in neural tissue was due to neural growth. This
139 neural growth was not exclusive to DSS damage since we also observed it when
140 feeding the flies Bleomycin and H_2O_2 (Fig. 1D,E, Fig. S2A,B). In contrast,
141 *Pseudomonas entomophila* infection led to a marked gut enlargement in our region of
142 interest, with neural tissue scaling accordingly. Because this expansion likely
143 approached the limit of neural growth, it prevented detection of any plasticity growth
144 beyond this scaling response (Fig. S2C). Overall, several forms of chemically induced
145 damage paradigms robustly trigger neural growth.
146
147 Tracheal terminal cells (TTCs) sprout in response to DSS, Bleomycin, H_2O_2, and
148 infectious pathogens (Medina et al., 2025; Perochon et al., 2021; Tamamouna et al.,
149 2021), so we examined their behavior in the anterior midgut. This region showed
150 sparse tracheation, which remained unchanged after DSS feeding, indicating that
151 TTCs in this area were unresponsive to gut damage (Fig. S3A, B). Moreover, TTC
152 morphology did not match the extent of neural growth, suggesting that they do not
153 serve as a scaffold for neural tissue growth in this area.
154
155 We next explored the stability of this neural plasticity and conducted recovery
156 experiments (Fig. 1F). While DSS feeding increased the neural tissue (C versus DSS),
157 a 4-day recovery period (DSS + Rec) reverted the amount of neural tissue to levels as
158 those of control flies (C + Rec). Consistent with this observation, a clear reversal of
159 neural growth was observed when comparing flies dissected after the DSS treatment
160 (DSS) and those dissected after the recovery phase (DSS + Rec). No differences were
161 observed between control flies (C versus C + Rec).
162
163 In summary, these experiments indicate that the intact neural tissue innervating the
164 digestive tube is plastic and responds to damage with growth. This neural growth is
165 reversible after a recovery period, as the gut returns to homeostasis after injury.
166 Importantly, these observations were validated with two independent neural drivers
167 (*GMR51F12-GAL4*, Fig. 1 and *nSyb.S-GAL4*, Fig. S3C).
168

ISC proliferation does not mediate neural plasticity.

To determine whether ISC proliferation drove DSS-induced neural growth, we first confirmed that DSS feeding increased ISC division in the anterior midgut, as shown by elevated phospho-histone H3 (PH3) signal (Fig. 2A) and lineage tracing using ReDDM (Antonello et al., 2015) (Fig. 2B) (see Materials and Methods). To test causality, we blocked ISC cell division during DSS feeding using a combination of a *Cdk1* null allele (*Cdk1*^{null}) and a temperature-sensitive allele (*Cdk*$^{1E1-24}$) (Rodríguez et al., 2024) (Fig. 2C). Neural growth remained unaffected by the proliferation block (Fig. 2D), indicating that ISC division is not required for DSS-induced neural plasticity.

Gut-derived ROS stimulates neural plasticity

DSS feeding results in epithelial damage, causing cell death and an increase in ROS levels (Wu et al., 2012)(Fig. S4A). To test the contribution of ROS levels to neural growth, we co-fed flies with DSS and the ROS inhibitor N-acetyl cysteine (NAC). Neural growth was reduced in DSS + NAC flies and comparable to control + NAC levels (Fig. 2E), indicating that DSS-dependent ROS promotes neural plasticity. This finding aligns with evidence that ROS supports structural plasticity (Oswald et al., 2018).

It has been recently shown that ROS from midgut epithelial cells promotes the secretion of diuretic hormone 31 (Dh31) from anterior EE cells and that Dh31 binds Dh31 receptor (Dh31-R) to mediate tracheal remodeling (Medina et al., 2025). To test whether ROS-induced Dh31 signaling mediates the increase in neural tissue observed after DSS feeding, we verified that Dh31-R was expressed in neurons in the HCG (Medina et al., 2025)(Fig. S4C). We analyzed *Dh31* mutants and flies with neuronal knockdown of its receptor, *Dh31-R* (Fig. S4D-G). Baseline innervation was unaffected in either condition (Fig. S4D,F). DSS feeding induced a comparable increase in neural tissue in *Dh31* homozygous mutants and heterozygous controls (Fig. S4E), as well as in *Dh31R* knockdown flies (Fig. S4G). These results indicate that the DSS-dependent, ROS-induced neural plasticity occurs independently of the Dh31/Dh31-R pathway.

Reversal of neural growth as the gut returns to homeostasis is not caspase dependent.

202 We were curious about the mechanisms controlling neural growth reversal during
203 recovery. Axon pruning can take place either through axon retraction or degeneration
204 (Luo and O'Leary, 2005). During developmental remodeling, dendritic arborizing (da)
205 sensory neurons ddaC degenerate (Williams and Truman, 2005) using local caspase
206 activation to direct dendrite engulfment (Williams et al., 2006). To assess whether
207 caspases mediated neural growth reversal, we inhibited apoptosis in neurons by
208 overexpressing Diap1. Reversal still occurred (Fig. S5), suggesting that this process
209 may result from axon retraction rather than caspase-dependent mechanisms.
210
211 **Neural plasticity is exclusive to females and is actively suppressed when female**
212 **neurons are masculinized.**
213 Interestingly, males did not exhibit neural growth following DSS treatment (Fig. 3A)
214 despite a DSS-dependent increase in ROS (Fig. S4B) and reduced viability
215 (Amcheslavsky et al., 2009). To investigate whether this neural growth was exclusive
216 to female neurons, we aimed to create female individuals with masculinized neurons.
217 Most sex differences in *Drosophila* arise from the female-specific expression of the
218 *Sex lethal* gene (*Sxl*), which codes for an RNA-binding protein (Bell et al., 1988). Sxl
219 induces the alternative splicing of the *transformer* (*tra*) gene, generating the female
220 fate-determining TraF protein only in females (Belote et al., 1989; Boggs et al., 1987;
221 Inoue et al., 1990; Sosnowski et al., 1989). We first confirmed that neurons in the HCG
222 expressed the female-specific alternative splicing variant of *tra* while males didn't (Fig.
223 3B,C) (Hérault et al., 2024). Subsequently, we proceeded to masculinize neurons in
224 females by means of *tra* downregulation with RNAi during development (Fig. 3D). We
225 confirmed that the presence of the *UAS-Dcr2* transgene did not affect the response of
226 wild-type females to DSS, and thus, the expected increase in neural tissue was
227 observed. Interestingly, DSS feeding did not have any effect on masculinized females,
228 and the amount of neural tissue was not significantly different between control and
229 DSS-fed flies. In addition, DSS-fed masculinized females displayed significantly less
230 neural tissue than DSS-fed control flies, aligning with the absence of neural growth in
231 masculinized females.
232
233 We also carried out the reverse experiment and attempted to confer plasticity to male
234 neurons by feminizing them through developmental *Sxl* overexpression (Fig. 3E) (Bell
235 et al., 1991). In this case, the DSS treatment had no effect on feminized males, and

we did not observe the neural growth we expected to see for a successfully feminized male. Moreover, both control and DSS-fed feminized males showed less amount of neural tissue than wild-type males. These results indicate that neuronal Sxl overexpression in males is not sufficient to induce damage-responsive plasticity and may even impair neural tissue growth in our context.

These findings reveal a previously unrecognized sex-specific mechanism of neural plasticity in the fly gut, where female neurons exhibit a unique capacity for damage-induced growth that is actively suppressed by masculinization. In addition, the lack of neural growth in males following DSS-induced gut damage suggests that neural plasticity is limited in males compared to females.

Female-specific neural plasticity impacts gut physiology and viability

To address the functional impact of neural plasticity, we carried out defecation assays both after DSS treatment and after recovery treatment. We observed that DSS feeding caused a robust increase in defecation (Fig. 4A,B) (see Material and Methods). After a 4-day recovery period on sucrose (Fig. 4A), defecation in flies previously exposed to DSS (DSS + Rec) remained significantly higher than in control flies (C + Rec), although neural tissue increase reverts in these conditions (Fig. 1F). When the recovery period was performed on standard food (Fig. 4B), defecation in DSS-treated flies (DSS + Rec) was not significantly different from controls (C + Rec). Although the difference under this condition did not reach statistical significance, the values still showed a mild upward trend in DSS-recovered flies, which is consistent with the expectation that physiology may not be fully restored but approaches near-normal levels. These observations suggest that standard food promotes recovery of the digestive tube, and that normalization of defecation requires coordinated restoration of both neural and gut homeostasis.

However, whether neural plasticity contributes to the increased defecation and its potential protective role remained unclear. To address this, we masculinized female neurons to block their DSS-induced plasticity. This manipulation markedly suppressed the defecation increase after DSS feeding (Fig. 4C), indicating that neural plasticity is required for this physiological response. Independently, lifespan analysis showed that eliminating neural plasticity (i.e. masculinizating neurons) further reduced the survival

of DSS-fed female flies (Fig. 4D), suggesting that the plastic response also provides a protective benefit.

Together, these results reveal two different effects of neural plasticity under DSS challenge, even though how the increase in neural tissue contributes to these behaviors and whether they are connected remains unknown. Nonetheless, they highlight the importance of neural plasticity in shaping the physiological response to gut damage.

The *Drosophila* gut and its innervation as a model to investigate neural plasticity and the role of sex in its regulation

This system enables the study of both structural growth and retraction phases of adult intact neural tissue in response to damage, capturing the dynamic nature of plasticity. In addition, we uncovered a clear sexual dimorphism: neural growth is absent in males and suppressed in masculinized female neurons. However, feminizing male neurons was not sufficient to induce plasticity.

Two complementary directions emerge for understanding this dimorphism. One line of inquiry concerns sex-specific gene expression that may underlie the differential plasticity. Sex differences in genes regulating ROS production and/or ROS-responsive signalling pathways could drive the female-specific neural growth observed in response to gut damage. For the latter, candidate pathways include TOR and InR/PI3K/Akt, which regulate neural regrowth during developmental remodeling in flies (Sanal et al., 2023; Yaniv and Schuldiner, 2016) and mammalian regeneration (Lund-Ricard et al., 2020). Other molecules downstream of ROS are Umpaired (Upd) cytokines, such as Upd3 (Santabárbara-Ruiz et al., 2015), which could link tissue damage to neural plasticity (see below).

The other direction focuses on the influence of surrounding tissues on neural plasticity. The failure of feminized male neurons to elicit growth in response to damage implies that neuronal identity alone is not enough—sex-specific cues from surrounding tissues such as the gut epithelium, visceral muscle, tracheal cells or Malpighian tubules may be necessary to support or trigger neural growth. Indeed, Upd3 can be secreted by damaged gut epithelial cells, visceral muscle or Malpighian tubules, leading directly or

indirectly to ISC proliferation (Buchon et al., 2010, 2009a, 2009b; Jiang et al., 2009; Lin et al., 2010; Liu et al., 2024; Medina et al., 2022; Osman et al., 2012; Tian et al., 2015). Recent studies show that neurons can respond directly to glia-derived Upd3, which modulates neuronal structure (Sodders et al., 2025), and indirectly to gut-derived Upd2/3 via glial intermediates, which influences neuronal function (Malita et al., 2025). Together, these initial insights raise the possibility that the neural plasticity observed after DSS feeding may be shaped by Unpaired ligands present in the gut microenvironment. Similarly, reversal of neural growth during recovery may involve repulsive cues such as Ephrins, Slits, or Semaphorins, potentially transiently expressed in tissues of the digestive tube environment in females, thereby mediating axon retraction in a manner reminiscent of classic axon-guidance mechanisms (Luo and O'Leary, 2005).

Building on evidence that sex influences organ formation and physiology (Mank and Rideout, 2021), the results presented here establish the *Drosophila* gut and its innervation as a model for elucidating how sex shapes neural plasticity of intact neural tissue in response to damage. Understanding these mechanisms could guide the development of sex-specific therapeutic strategies for neural repair.

MATERIALS AND METHODS

Fly stocks

The following fly lines were used: *GMR51F12-GAL4* (BDSC:58685), *nSyb.S-GAL4* (BDSC: 51635), *UAS-Flybow.1.1B* (used as 10xUAS-CD8::GFP, BDSC: 56802, 56803), *DSRF.Term-GAL4* (BDSC: 25753), *esg-GAL4* (a gift from M. Milán, unknown insertion), *UAS-mCD8::GFP* (BDSC:5130), *UAS-H2B::RFP* (a gift from J. Morante), *tubP-GAL80^{ts}* (BDSC: 7017), *Cdk1^{null}* (BDSC: 6643), *Cdk$^{1E1–24}$* (BDSC: 6641), *Dh31^{attP}* (BDSC: 84490), *UAS-Dh31-R RNAi TRIPJF01945* (UAS-Dh31-R RNAi, BDSC: 25925), *Dh31-R$^{2A-Gal4}$* (BDSC: 84626), *UAS-Diap1* (BDSC: 15310), *traF-GAL4* (a gift from B. Hudry), *UAS-Dcr-2* (BDSC: 24650), *UAS-tra RNAi TRiPJF03132* (*UAS-tra RNAi*, BDSC: 28512), *UASp-Sxl.alt5-C8* (*UAS-Sxl*, BDSC: 58484). The list of complete genotypes is available in Supplementary Information.

Feeding protocols

337 For feeding assays, virgin females were collected and aged on standard media at 25ºC
338 for 3-4 days before undergoing mating for 24 h. The same procedure was carried out
339 when experiments were performed with males. Flies were recovered from the mating
340 and transferred in groups of 10 to an empty vial containing 5 pieces of 2cm × 2cm of
341 bench paper soaked with 500ml of the desired feeding solution. Flies were transferred
342 to a new vial with fresh feeding paper every day for the specified number of days prior
343 to dissection. The feeding protocol was always done at 29ºC, all feeding treatments
344 were administered in 5% sucrose (S7903, Sigma Aldrich), and flies fed with sucrose
345 alone served as the control (C) condition unless otherwise stated. Flies were fed with
346 DSS (42867, Sigma Aldrich) at 6% w/v for 4 days. For the SMURF assay, the last
347 control and DSS feeding solutions prior to the day of dissection were laced with Brilliant
348 Blue FCF (80717, Supelco) at 2.5% w/v. Bleomycin (BL7216, Sigma Aldrich) was
349 administered at 50 µg ml^{-1} for 3 days, H_2O_2 (1072100250, Supelco) at 1% for 4 days,
350 and *Pseudomonas entomophila* (*Pe*) at an OD_{600}=25 for 16 h. For NAC (A7250, Sigma
351 Aldrich) co-treatment, flies were fed with 1,2 mM NAC in 5% sucrose (Control + NAC)
352 or 6% DSS + 1,2 mM NAC in 5% sucrose (DSS + NAC) for 4 days. For recovery (Rec)
353 experiments, after the feeding protocol, C and DSS-fed flies were each transferred to
354 vials with 5% sucrose for 4 days (C + Rec ; DSS + Rec). To carry out comparisons
355 within the same cohort of flies, a subset of flies was dissected after the feeding
356 protocol, and the rest after the recovery period.
357
358 **Temperature-sensitive assays**
359 To visualize the amount of proliferation taking place exclusively during the four days
360 of the feeding protocol, we set ReDDM-based crosses (Antonello et al., 2015). This
361 lineage tracing approach uses the Gal80 temperature-sensitive allele (*Gal80^{ts}*), which
362 inhibits GAL4 transcription at permissive temperature (19ºC) and allows it at the
363 restrictive one (29ºC) (McGuire et al., 2003), and *esg-GAL4* to label ISCs and EBs.
364 Crosses were grown and flies were kept at 17°C to ensure Gal80^{ts} repression until
365 adult mated female flies were shifted to 29°C to inactivate Gal80 and carry out the
366 feeding protocol. To block ISC proliferation during the feeding protocol, *Cdk1^{null}/*
367 *Cdk$^{1E1–24}$* flies were grown, aged, and mated at 17ºC, Cdk1 function was abrogated
368 once the flies were transferred to 29ºC (Rodriguez et al., 2024) during the DSS feeding
369 protocol.
370

371 **Dissection and immunostaining**

372 To obtain the gut, flies were dissected in PBS. Adult animals had their heads cut off
373 with scissors by the neck, their abdomens were pulled apart from the thorax, and
374 opened to extract the gut. With this procedure, the digestive tube was severed well
375 above the crop duct. Once the fat and ovaries were removed, the gut was handled by
376 its posterior end and transferred to PBS in a well drawn onto a poly-L-lysine-coated
377 slide (P1524, Merck) using hydrophobic silicone (Flowsil, Intek Adhesives). In cases
378 where the anterior part of the midgut had to be repositioned, we manipulated the gut
379 from the crop to avoid touching the digestive tube. Guts were fixed at room
380 temperature for 30 min in 4% PFA in PBS. Washes were done with PBS-T (PBS,
381 0.25% Triton X-100). To label the muscle or nuclei, guts were incubated at room
382 temperature for 30 min with Alexa Fluor™ 635 Phalloidin (1/400, A34054, Invitrogen)
383 or Hoechst 33258 (1/1000, H3569, Invitrogen), respectively, in PBS-T. A final wash
384 with PBS was done before mounting. When antibodies were used, primaries were
385 incubated overnight at 4ºC, and secondaries were incubated at room temperature for
386 2–3 h. The following antibodies were used: rat-anti-Elav (1/100, 7E8A10, DSHB),
387 mouse-anti-Discs large (1/50, 4F3, DSHB), rabbit-anti-PH3 (1/1000, 06-570, EMD
388 Milipore), rabbit-anti-DsRed (1/200, 632496, Clontech), chicken-anti-GFP (1/800,
389 ab13970, Abcam), Alexa Fluor™ 568 goat-anti-rat, Alexa Fluor™ 488 goat-anti-
390 mouse, Alexa Fluor™ 488 goat-anti-rabbit, Alexa Fluor™ 568 goat-anti-rabbit, Alexa
391 Fluor™ 488 goat-anti-chicken (1/500, A11077, A11001, A11008, A11011, A11039,
392 Life Technologies). Samples were mounted in VECTASHIELD® PLUS Antifade
393 Mounting (H-1900-10, Vector Laboratories).

394

395 **ROS detection**

396 C and DSS-fed guts were dissected in Schneider's medium (50146, Sigma Aldrich)
397 and placed on poly-L-lysine-coated slides. Tissues were incubated in CM-H_2DCFDA
398 (C6827, Invitrogen) at 2 μM in Schneider's medium for 30 min in the dark, then washed
399 three times in Schneider's medium before imaging. Dissection time was limited to 15
400 min for each experimental group, and imaging was performed within 45 min of
401 dissection.

402

403 **Defecation assay**

404 Flies under analysis were starved for 1 h in empty vials. Subsequently, 20–25 flies
405 were introduced into fly cages positioned over a 60-mm Petri dish containing a central
406 5 × 5 mm piece of grape-juice agar with 2.5% (w/v) Brilliant Blue FCF (Supelco,
407 80717). Flies were kept at 29 °C for 12 h in constant darkness before quantification of
408 the fecal spots.
409
410 **Lifespan experiments**
411 Lifespan analysis of females aged and mated started on the 1st day of the feeding
412 protocol and after that continued for 8 additional days on 5% sucrose. Flies were
413 placed in groups of maximum 10 per vial, and transferred to new feeding vials every
414 day.
415
416 **Microscopy**
417 Samples were imaged using a Zeiss LSM 880 confocal microscope (Zeiss, Germany)
418 equipped with a 25X 0.8 glycerol immersion media objective and an Argon and a
419 HeNe633 lasers. For neural network analysis, to consistently image the same region
420 in each gut, we used the end of the proventriculus as a positional landmark and
421 captured the gut section that fit within the visual field of the 25X objective at 0.8
422 magnification, which in our setup generated images of 566,79 μm^2. As quality control
423 for dissection, only guts with an intact HCG were considered since this ganglion
424 contains the cell bodies of many of the neurons innervating the anterior midgut. Stacks
425 of images were acquired with a pixel size of 0.55x0.55x1um (xyz) and a pixel dwell
426 time of 2.05us.
427
428 **Image processing and quantification based on images**
429 Images were processed with Fiji (version ImageJ 1.53c, (Schindelin et al., 2012) and
430 figures assembled using Adobe Illustrator (Adobe, San Jose, CA).
431 *Quantification of neural tissue and gut parameters:* The channel with the neuron
432 staining was filtered in 3D (Ollion et al., 2013) first with the maximum filter and then
433 with the minimum one, with a radius of 3.3um in x and y and 2um in z, in both filters.
434 Then the filtered stack was processed using the Tubeness plugin (sigma = 0.66) (Sato
435 et al., 1998). Finally, images were binarized using the Bernsen's AutoLocal threshold
436 method (radius = 2) (Bernsen, 1986). The resulting binary stack was analyzed first
437 with the 3D Object Counter function to obtain the total neuronal network volume (mm^3).

438 The channel with the gut staining was processed by background subtraction and then
439 thresholder using the Li's method (Li and Lee, 1993). The resulting binary stack was
440 analyzed with the 3D Object Counter function to obtain the volume of the gut.
441 *Other quantifications on images:* The number of Elav/Hoechst positive nuclei in the
442 HCG was counted from the confocal stack using the 3D Object Counter plugin. The
443 number of TTC nuclei was counted by hand from the confocal stack maximum
444 projection. TTCs volume was obtained using the same procedure as for neural tissue
445 quantification. The number of PH3/ Hoechst positive nuclei in the midgut was counted
446 directly under the confocal microscope. For quantification of cumulative proliferation
447 using ReDDM, xyz stacks of half the gut were taken and z-projected. The Hoechst
448 signal was manually outlined to measure the gut area. To quantify the area of GFP
449 signal from mCD8::GFP-labeled cells (representing ISCs and EBs resulting from ISCs
450 divisions) a Gaussian Blur filter (radius = 2.0) was applied. The image was then
451 thresholded using the "MaxEntropy" algorithm (Kapur et al., 1985), and finally, the
452 GFP-positive regions larger than $10\mu m^2$ were quantified. The GFP area was
453 represented as a percentage of the total area. To quantify the number of differentiated
454 ECs, the total number of ReDDM cells was quantified manually using the H2B::RFP
455 nuclear signal, the presence or absence of cytoplasmic mCD8::GFP was tracked to
456 calculate the percentage of differentiated ECs. For ROS signal analysis, the same
457 region used for neural network evaluation was imaged. Z-projections combining 15
458 optical sections were generated using maximum intensity to capture the epithelial
459 signal. For each gut image, mean pixel intensity was quantified in two distinct areas to
460 account for variability across the imaged gut region.
461
462 **Other quantifications**
463 *SMURF assay*: on the 4th day of the DSS feeding protocol, we assessed the proportion
464 of surviving flies that were positive for the SMURF phenotype. Ten tubes with 10 flies
465 each were used in each of three biologically independent replicates.
466 *Defecation assay:* After incubation, the Petri dish was removed, and the four quadrants
467 of the dish were photographed separately under a stereomicroscope. Blue fecal spots
468 in each quadrant were manually counted using ImageJ and normalized by the total
469 number of flies in the cage. Thus, the value obtained represented fecal spots per
470 quadrant/total flies in the cage. Each quadrant was treated as an independent

technical replicate. This approach increased the number of measurements per biological replicate, thereby improving the statistical power of the analysis while ensuring complete and accurate counting of all fecal deposits. Flies from the same cohort were used in experiments where defecation assays were carried out after DSS treatment and after recovery treatment.

Lifespan experiments: dead flies were counted every 24 h before being transferred to a new feeding vial.

Statistics

Data analysis was carried out using Prism 6 (GraphPad Software Inc., San Diego, CA) and Statgraphics Centurion version 18 (Statgraphics Technologies Inc., The Plains, VA). Table S1 provides statistical details (sample size for each condition, definition of values, statistical test, comparisons and p values) for each main and supplementary figure. All tests are two-tailed. For data shown in box plots, the median is given between the first and third quartiles (ends of the box). Whiskers represent the maximum and minimum values of the data. Bar graphs display the mean, with error bars representing the standard deviation.

For the amount of neural tissue and TTCs tissue: To analyze the effect of the treatment on neural tissue volume and TTCs tissue volume, analysis of covariance (ANCOVA) was performed. The dependent variable was neural tissue volume or TTCs tissue volume, the fixed factor was the treatment, and the covariate was gut volume (Fig. 1B,D-F; Fig. 2D,E; Fig. 3A,D,E; Fig. S1A-D,G-H, ; Fig. S2A-C; Fig. S3B-C; Fig. S4D-G; Fig. S5).

For other quantifications: For pairwise comparisons of data sets following a normal distribution (Fig. 1C, Fig. S4A,B), the unpaired t-test was performed. For pairwise comparisons of data sets not following a normal distribution, we used the non-parametric Mann-Whitney test (Fig. 2A-C; Fig. 4A-C; Fig. S3A).

For lifespan experiments: survival distributions were compared using the non-parametric log-rank test (Kaplan and Meier, 1958), which accounts for censored data. To correct for multiple comparisons, the Holm–Bonferroni method was applied to control the family-wise error rate (Holm, 1979).

ACKNOWLEDGEMENTS

We thank M. Corominas, C. Estella, A. Gontijo, C. González, A. González-Reyes, B. Hudry, M. Llimargas, M. Milán, J. Morante, F. Serras, M. Silies, H. Stocker, BDSC, and DSHB for reagents and members of the Corominas' and Serras' laboratories for insightful discussions. We are grateful to: Q. Zhu, P. Longas, and O. Ramirez for their assistance with early pilot experiments that helped shape this research; PG. Camara, P. Nicodemus, V. Pisarenco, and J. Rozas for help in exploring the use of a metric-geometry framework (CAJAL) to describe morphology changes in the anterior midgut neural network; J. Vila for help with *Pe* feeding experiments, and C. Herrera for informatic support. We are indebted to our colleagues F. Cebrià, M. Corominas, F. Serras, M. Valls, T. Adell, C. González-Estevez, L. di Croce, L. Morey, B. Payer, and the CCiTUB technological platform for their invaluable support and encouragement during this project.

COMPETING INTERESTS

The authors declare no competing interests.

AUTHOR CONTRIBUTIONS

Conceptualization: M.M.; Methodology: M.R-M., M.B., P.G., A.M., S.R., I.M-A., M.M.; Investigation: M.R-M., M.M.; Formal Analysis: M.R-M., P.G., A.M., S.R., I.M-A., M.M.; Validation: M.R-M., M.M.; Visualization: M.R-M., M.M.; Data Curation: M.R-M., M.M.; Resources: P.G., A.M., I.M-A.; Supervision: M.M.; Project Administration: M.M.; Funding Acquisition: M.M.; Writing – Original Draft: M.M. with contributions from all the authors; Writing- review and editing: M.M.

AI-assisted tools (ChatGPT, GTP-5) were used for language editing during manuscript preparation. All content generated by the AI was reviewed and edited by the authors, who take full responsibility for the final text.

FUNDING

This work was funded by the Spanish Ministerio de Ciencia e Innovación (grant PID2019-107340GB-I00) and Agència de Gestió d'Ajuts Universitaris i de Recerca of the Generalitat de Catalunya (2021SGR00293) to M.M. Work in I.M-A. was funded by an ERC Advanced Grant (ERCAdG 787470 "IntraGutSex"), a UKRI Horizon Europe guarantee grant (EPSRC-ERC EP/Y03298/1), MRC intramural funding and the

Francis Crick Institute, which receives its core funding from Cancer Research UK (FC001317 and FC001175), the UK Medical Research Council (FC001317 and FC001175), and the Wellcome Trust (FC001317 and FC001175).

DATA AND RESOURCE AVAILABILITY

All relevant data and details of resources can be found within the article and its supplementary information.

REFERENCES

Amcheslavsky, A., Jiang, J., Ip, Y.T., 2009. Tissue Damage-Induced Intestinal Stem Cell Division in Drosophila. Cell Stem Cell 4, 49–61. https://doi.org/10.1016/j.stem.2008.10.016

Antonello, Z.A., Reiff, T., Ballesta-Illan, E., Dominguez, M., 2015. Robust intestinal homeostasis relies on cellular plasticity in enteroblasts mediated by miR-8–Escargot switch. EMBO J. 34, 2025–2041. https://doi.org/10.15252/embj.201591517

Bell, L.R., Horabin, J.I., Schedl, P., Cline, T.W., 1991. Positive autoregulation of Sex-lethal by alternative splicing maintains the female determined state in Drosophila. Cell 65, 229–239. https://doi.org/10.1016/0092-8674(91)90157-T

Bell, L.R., Maine, E.M., Schedl, P., Cline, T.W., 1988. Sex-lethal, a Drosophila sex determination switch gene, exhibits sex-specific RNA splicing and sequence similarity to RNA binding proteins. Cell 55, 1037–1046. https://doi.org/10.1016/0092-8674(88)90248-6

Belote, J.M., McKeown, M., Boggs, R.T., Ohkawa, R., Sosnowski, B.A., 1989. Molecular genetics of *transformer* , a genetic switch controlling sexual differentiation in *Drosophila*. Dev. Genet. 10, 143–154. https://doi.org/10.1002/dvg.1020100304

Bentley, D., Toroian-Raymond, A., 1981. Embryonic and postembryonic morphogenesis of a grasshopper interneuron. J. Comp. Neurol. 201, 507–518. https://doi.org/10.1002/cne.902010404

Bernsen, J., 1986. Dynamic Thresholding of Gray Level Image. Proc. Int. Conf. Pattern Recognit. Berl. ICPR 86 1251–1255.

570 Boggs, R.T., Gregor, P., Idriss, S., Belote, J.M., McKeown, M., 1987. Regulation of
571 sexual differentiation in D. melanogaster via alternative splicing of RNA from
572 the transformer gene. Cell 50, 739–747. https://doi.org/10.1016/0092-
573 8674(87)90332-1
574 Bucher, D., Pflüger, H.-J., 2000. Directional sensitivity of an identified wind-sensitive
575 interneuron during the postembryonic development of the locust. J. Insect
576 Physiol. 46, 1545–1556. https://doi.org/10.1016/S0022-1910(00)00078-0
577 Buchon, N., Broderick, N.A., Chakrabarti, S., Lemaitre, B., 2009a. Invasive and
578 indigenous microbiota impact intestinal stem cell activity through multiple
579 pathways in *Drosophila*. Genes Dev. 23, 2333–2344.
580 https://doi.org/10.1101/gad.1827009
581 Buchon, N., Broderick, N.A., Kuraishi, T., Lemaitre, B., 2010. DrosophilaEGFR
582 pathway coordinates stem cell proliferation and gut remodeling following
583 infection. BMC Biol. 8, 152. https://doi.org/10.1186/1741-7007-8-152
584 Buchon, N., Broderick, N.A., Poidevin, M., Pradervand, S., Lemaitre, B., 2009b.
585 Drosophila Intestinal Response to Bacterial Infection: Activation of Host
586 Defense and Stem Cell Proliferation. Cell Host Microbe 5, 200–211.
587 https://doi.org/10.1016/j.chom.2009.01.003
588 Buchon, N., Osman, D., David, F.P.A., Yu Fang, H., Boquete, J.-P., Deplancke, B.,
589 Lemaitre, B., 2013. Morphological and Molecular Characterization of Adult
590 Midgut Compartmentalization in Drosophila. Cell Rep. 3, 1725–1738.
591 https://doi.org/10.1016/j.celrep.2013.04.001
592 Chen, J., Reiher, W., Hermann-Luibl, C., Sellami, A., Cognigni, P., Kondo, S.,
593 Helfrich-Förster, C., Veenstra, J.A., Wegener, C., 2016. Allatostatin A
594 Signalling in Drosophila Regulates Feeding and Sleep and Is Modulated by
595 PDF. PLOS Genet. 12, e1006346.
596 https://doi.org/10.1371/journal.pgen.1006346
597 Cirillo, C., Brihmat, N., Castel-Lacanal, E., Le Friec, A., Barbieux-Guillot, M., Raposo,
598 N., Pariente, J., Viguier, A., Simonetta-Moreau, M., Albucher, J.-F., Olivot, J.-
599 M., Desmoulin, F., Marque, P., Chollet, F., Loubinoux, I., 2020. Post-stroke
600 remodeling processes in animal models and humans. J. Cereb. Blood Flow
601 Metab. 40, 3–22. https://doi.org/10.1177/0271678X19882788
602 Cognigni, P., Bailey, A.P., Miguel-Aliaga, I., 2011. Enteric Neurons and Systemic
603 Signals Couple Nutritional and Reproductive Status with Intestinal

Homeostasis. Cell Metab. 13, 92–104. https://doi.org/10.1016/j.cmet.2010.12.010

Cui, X., Meiselman, M.R., Thornton, S.N., Yapici, N., 2024. A gut-brain-gut interoceptive circuit loop gates sugar ingestion in Drosophila. https://doi.org/10.1101/2024.09.02.610892

Gao, Z., Pang, Z., Chen, Y., Lei, G., Zhu, S., Li, G., Shen, Y., Xu, W., 2022. Restoring After Central Nervous System Injuries: Neural Mechanisms and Translational Applications of Motor Recovery. Neurosci. Bull. 38, 1569–1587. https://doi.org/10.1007/s12264-022-00959-x

Hérault, C., Pihl, T., Hudry, B., 2024. Cellular sex throughout the organism underlies somatic sexual differentiation. Nat. Commun. 15, 6925. https://doi.org/10.1038/s41467-024-51228-6

Holm, S., 1979. A Simple Sequentially Rejective Multiple Test Procedure. Scand. J. Stat. 6, 65–70.

Holsopple, J.M., Cook, K.R., Popodi, E.M., 2022. Enteroendocrine cell expression of split-GAL4 drivers bearing regulatory sequences associated with panneuronally expressed genes in Drosophila melanogaster. Open Access.

Howard, A.M., LaFever, K.S., Fenix, A.M., Scurrah, C.R., Lau, K.S., Burnette, D.T., Bhave, G., Ferrell, N., Page-McCaw, A., 2019. DSS-induced damage to basement membranes is repaired by matrix replacement and crosslinking. J. Cell Sci. 132, jcs226860. https://doi.org/10.1242/jcs.226860

Hyer, M.M., Phillips, L.L., Neigh, G.N., 2018. Sex Differences in Synaptic Plasticity: Hormones and Beyond. Front. Mol. Neurosci. 11, 266. https://doi.org/10.3389/fnmol.2018.00266

Inoue, K., Hoshijima, K., Sakamoto, H., Shimura, Y., 1990. Binding of the Drosophila Sex-lethal gene product to the alternative splice site of transformer primary transcript. Nature 344, 461–463. https://doi.org/10.1038/344461a0

Jenett, A., Rubin, G.M., Ngo, T.-T.B., Shepherd, D., Murphy, C., Dionne, H., Pfeiffer, B.D., Cavallaro, A., Hall, D., Jeter, J., Iyer, N., Fetter, D., Hausenfluck, J.H., Peng, H., Trautman, E.T., Svirskas, R.R., Myers, E.W., Iwinski, Z.R., Aso, Y., DePasquale, G.M., Enos, A., Hulamm, P., Lam, S.C.B., Li, H.-H., Laverty, T.R., Long, F., Qu, L., Murphy, S.D., Rokicki, K., Safford, T., Shaw, K., Simpson, J.H., Sowell, A., Tae, S., Yu, Y., Zugates, C.T., 2012. A GAL4-Driver

637 Line Resource for Drosophila Neurobiology. Cell Rep. 2, 991–1001.
638 https://doi.org/10.1016/j.celrep.2012.09.011
639 Jiang, H., Patel, P.H., Kohlmaier, A., Grenley, M.O., McEwen, D.G., Edgar, B.A.,
640 2009. Cytokine/Jak/Stat Signaling Mediates Regeneration and Homeostasis
641 in the Drosophila Midgut. Cell 137, 1343–1355.
642 https://doi.org/10.1016/j.cell.2009.05.014
643 Jiang, H., Tian, A., Jiang, J., 2016. Intestinal stem cell response to injury: lessons
644 from Drosophila. Cell. Mol. Life Sci. 73, 3337–3349.
645 https://doi.org/10.1007/s00018-016-2235-9
646 Kaplan, E.L., Meier, P., 1958. Nonparametric Estimation from Incomplete
647 Observations. J. Am. Stat. Assoc. 53, 457–481.
648 https://doi.org/10.1080/01621459.1958.10501452
649 Kapur, J.N., Sahoo, P.K., Wong, A.K.C., 1985. A new method for gray-level picture
650 thresholding using the entropy of the histogram. Comput. Vis. Graph. Image
651 Process. 29, 273–285. https://doi.org/10.1016/0734-189X(85)90125-2
652 Kenmoku, H., Ishikawa, H., Ote, M., Kuraishi, T., Kurata, S., 2016. A subset of
653 neurons controls the permeability of the peritrophic matrix and midgut
654 structure in *Drosophila* adults. J. Exp. Biol. jeb.122960.
655 https://doi.org/10.1242/jeb.122960
656 Kirby, E.D., Andrushko, J.W., Rinat, S., D'Arcy, R.C.N., Boyd, L.A., 2024.
657 Investigating female versus male differences in white matter neuroplasticity
658 associated with complex visuo-motor learning. Sci. Rep. 14, 5951.
659 https://doi.org/10.1038/s41598-024-56453-z
660 Ksiazek-Winiarek, D.J., Szpakowski, P., Glabinski, A., 2015. Neural Plasticity in
661 Multiple Sclerosis: The Functional and Molecular Background. Neural Plast.
662 2015, 1–11. https://doi.org/10.1155/2015/307175
663 Kuraishi, T., Kenmoku, H., Kurata, S., 2015. From mouth to anus: Functional and
664 structural relevance of enteric neurons in the Drosophila melanogaster gut.
665 Insect Biochem. Mol. Biol. 67, 21–26.
666 https://doi.org/10.1016/j.ibmb.2015.07.003
667 Lee, S., Stevens, C.F., 2007. General design principle for scalable neural circuits in a
668 vertebrate retina. Proc. Natl. Acad. Sci. 104, 12931–12935.
669 https://doi.org/10.1073/pnas.0705469104

670 Lemaitre, B., Miguel-Aliaga, I., 2013. The Digestive Tract of *Drosophila*
671 *melanogaster*. Annu. Rev. Genet. 47, 377–404.
672 https://doi.org/10.1146/annurev-genet-111212-133343
673 Li, C.H., Lee, C.K., 1993. Minimum cross entropy thresholding. Pattern Recognit. 26,
674 617–625. https://doi.org/10.1016/0031-3203(93)90115-D
675 Lin, G., Xu, N., Xi, R., 2010. Paracrine Unpaired Signaling through the JAK/STAT
676 Pathway Controls Self-renewal and Lineage Differentiation of Drosophila
677 Intestinal Stem Cells. J. Mol. Cell Biol. 2, 37–49.
678 https://doi.org/10.1093/jmcb/mjp028
679 Liu, Z., Zhang, H., Lemaitre, B., Li, X., 2024. Duox activation in Drosophila
680 Malpighian tubules stimulates intestinal epithelial renewal through a
681 countercurrent flow. Cell Rep. 43, 114109.
682 https://doi.org/10.1016/j.celrep.2024.114109
683 Lund-Ricard, Y., Cormier, P., Morales, J., Boutet, A., 2020. mTOR Signaling at the
684 Crossroad between Metazoan Regeneration and Human Diseases. Int. J.
685 Mol. Sci. 21, 2718. https://doi.org/10.3390/ijms21082718
686 Luo, L., O'Leary, D.D.M., 2005. AXON RETRACTION AND DEGENERATION IN
687 DEVELOPMENT AND DISEASE. Annu. Rev. Neurosci. 28, 127–156.
688 https://doi.org/10.1146/annurev.neuro.28.061604.135632
689 Mahar, M., Cavalli, V., 2018. Intrinsic mechanisms of neuronal axon regeneration.
690 Nat. Rev. Neurosci. 19, 323–337. https://doi.org/10.1038/s41583-018-0001-8
691 Malita, A., Skakkebaek, A.H., Kubrak, O., Chen, X., Koyama, T., Connolly, E.C.,
692 Ahrentloev, N., Andersen, D.S., Texada, M.J., Halberg, K., Rewitz, K., 2025.
693 Glia-mediated gut–brain cytokine signaling couples sleep to intestinal
694 inflammatory responses induced by oxidative stress. eLife 13, RP99999.
695 https://doi.org/10.7554/eLife.99999.3
696 Mank, J.E., Rideout, E.J., 2021. Developmental mechanisms of sex differences: from
697 cells to organisms. Development 148. https://doi.org/10.1242/dev.199750
698 Marianes, A., Spradling, A.C., 2013. Physiological and stem cell
699 compartmentalization within the Drosophila midgut. eLife 2, e00886.
700 https://doi.org/10.7554/eLife.00886
701 McGuire, S.E., Le, P.T., Osborn, A.J., Matsumoto, K., Davis, R.L., 2003.
702 Spatiotemporal Rescue of Memory Dysfunction in *Drosophila*. Science 302,
703 1765–1768. https://doi.org/10.1126/science.1089035

Medina, A., Bellec, K., Polcowñuk, S., Cordero, J.B., 2022. Investigating local and systemic intestinal signalling in health and disease with *Drosophila*. Dis. Model. Mech. 15, dmm049332. https://doi.org/10.1242/dmm.049332

Medina, A.B., Perochon, J., Tian, Y., Johnson, C.T., Holcombe, J., Ramesh, P., Polcowñuk, S., Yu, Y., Cordero, J.B., 2025. Neuroendocrine control of intestinal regeneration through the vascular niche in Drosophila. Dev. Cell 60, 3085-3101.e6. https://doi.org/10.1016/j.devcel.2025.06.036

Menon, K.P., Carrillo, R.A., Zinn, K., 2013. Development and plasticity of the *Drosophila* larval neuromuscular junction. WIREs Dev. Biol. 2, 647–670. https://doi.org/10.1002/wdev.108

Miguel-Aliaga, I., Jasper, H., Lemaitre, B., 2018. Anatomy and Physiology of the Digestive Tract of *Drosophila melanogaster*. Genetics 210, 357–396. https://doi.org/10.1534/genetics.118.300224

Min, S., Oh, Y., Verma, P., Whitehead, S.C., Yapici, N., Van Vactor, D., Suh, G.S., Liberles, S., 2021. Control of feeding by Piezo-mediated gut mechanosensation in Drosophila. eLife 10, e63049. https://doi.org/10.7554/eLife.63049

Murphy, T.H., Corbett, D., 2009. Plasticity during stroke recovery: from synapse to behaviour. Nat. Rev. Neurosci. 10, 861–872. https://doi.org/10.1038/nrn2735

Nudo, R.J., 2003. Functional and structural plasticity in motor cortex: implications for stroke recovery. Phys. Med. Rehabil. Clin. N. Am. 14, S57–S76. https://doi.org/10.1016/S1047-9651(02)00054-2

Olds, W.H., Xu, T., 2014. Regulation of food intake by mechanosensory ion channels in enteric neurons. eLife 3, e04402. https://doi.org/10.7554/eLife.04402

Ollion, J., Cochennec, J., Loll, F., Escudé, C., Boudier, T., 2013. TANGO: a generic tool for high-throughput 3D image analysis for studying nuclear organization. Bioinformatics 29, 1840–1841. https://doi.org/10.1093/bioinformatics/btt276

Osman, D., Buchon, N., Chakrabarti, S., Huang, Y.-T., Su, W.-C., Poidevin, M., Tsai, Y.-C., Lemaitre, B., 2012. Autocrine and paracrine unpaired signaling regulate intestinal stem cell maintenance and division. J. Cell Sci. 125, 5944–5949. https://doi.org/10.1242/jcs.113100

Oswald, M.C.W., Garnham, N., Sweeney, S.T., Landgraf, M., 2018. Regulation of neuronal development and function by ROS. FEBS Lett. 592, 679–691. https://doi.org/10.1002/1873-3468.12972

738 Perochon, J., Yu, Y., Aughey, G.N., Medina, A.B., Southall, T.D., Cordero, J.B., 2021.
739 Dynamic adult tracheal plasticity drives stem cell adaptation to changes in
740 intestinal homeostasis in Drosophila. Nat. Cell Biol. 23, 485–496.
741 https://doi.org/10.1038/s41556-021-00676-z
742 Petersen, E.D., Sharkey, E.D., Pal, A., Shafau, L.O., Zenchak-Petersen, J., Peña,
743 A.J., Aggarwal, A., Prakash, M., Hochgeschwender, U., 2022. Restoring
744 Function After Severe Spinal Cord Injury Through BioLuminescent-
745 OptoGenetics. Front. Neurol. 12, 792643.
746 https://doi.org/10.3389/fneur.2021.792643
747 Petsakou, A., Liu, Yifang, Liu, Ying, Comjean, A., Hu, Y., Perrimon, N., 2023.
748 Cholinergic neurons trigger epithelial Ca2+ currents to heal the gut. Nature
749 623, 122–131. https://doi.org/10.1038/s41586-023-06627-y
750 Prosperini, L., Piattella, M.C., Giannì, C., Pantano, P., 2015. Functional and
751 Structural Brain Plasticity Enhanced by Motor and Cognitive Rehabilitation in
752 Multiple Sclerosis. Neural Plast. 2015, 1–12.
753 https://doi.org/10.1155/2015/481574
754 Rera, M., Clark, R.I., Walker, D.W., 2012. Intestinal barrier dysfunction links
755 metabolic and inflammatory markers of aging to death in Drosophila. Proc.
756 Natl. Acad. Sci. U. S. A. 109, 21528–21533.
757 https://doi.org/10.1073/pnas.1215849110
758 Rodríguez, A., Foronda, D., Córdoba, S., Felipe-Cordero, D., Baonza, A., Miguez,
759 D.G., Estella, C., 2024. Cell proliferation and Notch signaling coordinate the
760 formation of epithelial folds in the *Drosophila* leg. Development 151,
761 dev202384. https://doi.org/10.1242/dev.202384
762 Sampaio-Baptista, C., Sanders, Z.-B., Johansen-Berg, H., 2018. Structural Plasticity
763 in Adulthood with Motor Learning and Stroke Rehabilitation. Annu. Rev.
764 Neurosci. 41, 25–40. https://doi.org/10.1146/annurev-neuro-080317-062015
765 Sanal, N., Keding, L., Gigengack, U., Michalke, E., Rumpf, S., 2023. TORC1
766 regulation of dendrite regrowth after pruning is linked to actin and exocytosis.
767 PLOS Genet. 19, e1010526. https://doi.org/10.1371/journal.pgen.1010526
768 Santabárbara-Ruiz, P., López-Santillán, M., Martínez-Rodríguez, I., Binagui-Casas,
769 A., Pérez, L., Milán, M., Corominas, M., Serras, F., 2015. ROS-Induced JNK
770 and p38 Signaling Is Required for Unpaired Cytokine Activation during

771 Drosophila Regeneration. PLOS Genet. 11, e1005595.
772 https://doi.org/10.1371/journal.pgen.1005595
773 Sato, Y., Nakajima, S., Shiraga, N., Atsumi, H., Yoshida, S., Koller, T., Gerig, G.,
774 Kikinis, R., 1998. Three-dimensional multi-scale line filter for segmentation
775 and visualization of curvilinear structures in medical images. Med. Image
776 Anal. 2, 143–168. https://doi.org/10.1016/S1361-8415(98)80009-1
777 Schindelin, J., Arganda-Carreras, I., Frise, E., Kaynig, V., Longair, M., Pietzsch, T.,
778 Preibisch, S., Rueden, C., Saalfeld, S., Schmid, B., Tinevez, J.-Y., White, D.J.,
779 Hartenstein, V., Eliceiri, K., Tomancak, P., Cardona, A., 2012. Fiji: an open-
780 source platform for biological-image analysis. Nat. Methods 9, 676–682.
781 https://doi.org/10.1038/nmeth.2019
782 Sodders, M., Das, A., Bai, H., 2025. Glial peroxisome dysfunction induces axonal
783 swelling and neuroinflammation in *Drosophila*. G3 Genes Genomes Genet.
784 15, jkae243. https://doi.org/10.1093/g3journal/jkae243
785 Sosnowski, B.A., Belote, J.M., McKeown, M., 1989. Sex-specific alternative splicing
786 of RNA from the transformer gene results from sequence-dependent splice
787 site blockage. Cell 58, 449–459. https://doi.org/10.1016/0092-8674(89)90426-
788 1
789 Tamamouna, V., Rahman, M.M., Petersson, M., Charalambous, I., Kux, K., Mainor,
790 H., Bolender, V., Isbilir, B., Edgar, B.A., Pitsouli, C., 2021. Remodelling of
791 oxygen-transporting tracheoles drives intestinal regeneration and
792 tumorigenesis in Drosophila. Nat. Cell Biol. 23, 497–510.
793 https://doi.org/10.1038/s41556-021-00674-1
794 Tedeschi, A., Bradke, F., 2017. Spatial and temporal arrangement of neuronal
795 intrinsic and extrinsic mechanisms controlling axon regeneration. Curr. Opin.
796 Neurobiol. 42, 118–127. https://doi.org/10.1016/j.conb.2016.12.005
797 Tian, A., Morejon, V., Kohoutek, S., Huang, Y., Deng, W., Jiang, J., 2022. Damage-
798 induced regeneration of the intestinal stem cell pool through enteroblast
799 mitosis in the *Drosophila* midgut. EMBO J. 41, e110834.
800 https://doi.org/10.15252/embj.2022110834
801 Tian, A., Shi, Q., Jiang, A., Li, S., Wang, B., Jiang, J., 2015. Injury-stimulated
802 Hedgehog signaling promotes regenerative proliferation of *Drosophila*
803 intestinal stem cells. J. Cell Biol. 208, 807–819.
804 https://doi.org/10.1083/jcb.201409025

Titos, I., Juginović, A., Vaccaro, A., Nambara, K., Gorelik, P., Mazor, O., Rogulja, D., 2023. A gut-secreted peptide suppresses arousability from sleep. Cell 186, 1382-1397.e21. https://doi.org/10.1016/j.cell.2023.02.022

Turtzo, L.C., McCullough, L.D., 2008. Sex Differences in Stroke. Cerebrovasc. Dis. 26, 462–474. https://doi.org/10.1159/000155983

Weaver, L.N., Ma, T., Drummond-Barbosa, D., 2020. Analysis of Gal4 Expression Patterns in Adult *Drosophila* Females. G3 GenesGenomesGenetics 10, 4147–4158. https://doi.org/10.1534/g3.120.401676

Williams, D.W., Kondo, S., Krzyzanowska, A., Hiromi, Y., Truman, J.W., 2006. Local caspase activity directs engulfment of dendrites during pruning. Nat. Neurosci. 9, 1234–1236. https://doi.org/10.1038/nn1774

Williams, D.W., Truman, J.W., 2005. Cellular mechanisms of dendrite pruning in *Drosophila* : insights from in vivo time-lapse of remodeling dendritic arborizing sensory neurons. Development 132, 3631–3642. https://doi.org/10.1242/dev.01928

Wu, S.-C., Liao, C.-W., Pan, R.-L., Juang, J.-L., 2012. Infection-Induced Intestinal Oxidative Stress Triggers Organ-to-Organ Immunological Communication in Drosophila. Cell Host Microbe 11, 410–417. https://doi.org/10.1016/j.chom.2012.03.004

Yang, C., Merlin, D., 2024. Unveiling Colitis: A Journey through the Dextran Sodium Sulfate-induced Model. Inflamm. Bowel Dis. 30, 844–853. https://doi.org/10.1093/ibd/izad312

Yaniv, S.P., Schuldiner, O., 2016. A fly's view of neuronal remodeling. WIREs Dev. Biol. 5, 618–635. https://doi.org/10.1002/wdev.241

Yu, C., An, Z., Zhao, W., Wang, W., Gao, C., Liu, S., Wang, J., Wu, J., 2015. Sex Differences in Stroke Subtypes, Severity, Risk Factors, and Outcomes among Elderly Patients with Acute Ischemic Stroke. Front. Aging Neurosci. 7. https://doi.org/10.3389/fnagi.2015.00174

FIGURE LEGENDS

Fig. 1. Neural plasticity induced by gut damage resolves after recovery. A) Drawing of the adult gut with two areas of interest highlighted and corresponding confocal Z-projections. The square box region corresponds to the area above the proventriculus (pv) and the image shows neuronal nuclei (magenta, anti-Elav) and

839 neuronal membrane (grey, GFP) of the HCG. Autofluorescence of the peritrophic
840 membrane lining the gut in this region is observed. The rectangular box region
841 corresponds to the area of the anterior midgut imaged in subsequent analyses and the
842 images show neuronal processes (grey, GFP) and muscle fibers (grey, Phalloidin). B)
843 Detailed schematic outlining the experiment in the panel, with rectangles representing
844 1 day each and reflecting the age of the flies (brown) and the duration of the feeding
845 protocol (purple) or any other additional period after that (light purple, like in panel F).
846 This type of schematic is used throughout the figures to describe the experiment
847 carried out. Confocal Z-projections of neuronal processes innervating the anterior
848 midgut of control (C) and DSS-fed (DSS) females and quantification of neural tissue.
849 Red outline in the box plots or bar graphs indicates female. C) Confocal Z-projections
850 of the HCG of C and DSS-fed females stained with Hoechst (grey, which also
851 accumulates in some tracheal branches) and showing neuronal nuclei (magenta, anti-
852 Elav). Quantification of neuronal nuclei in the HCG of C and DSS-fed females. D)
853 Quantification of neural tissue in C and Bleomycin (Bleo)-fed females. E)
854 Quantification of neural tissue in C and H_2O_2-fed females. F) Schematic of the feeding
855 protocol and recovery period. Quantification of neural tissue after the feeding protocol
856 and after the recovery period (Rec). Scale bar 50 μm. Statistical significance is
857 indicated as follows: * $p < 0.05$, ** $p < 0.01$, *** $p < 0.001$, ns = not significant. Gut
858 schematic from *BioRender.com*.
859
860 **Fig. 2. Neural plasticity does not depend on ISC proliferation but on gut-derived**
861 **ROS.** A) Quantification of PH3/Hoechst positive cells in the anterior and the whole
862 midgut in C and DSS-fed females. B) Schematic showing activation of ReDDM lineage
863 tracing during the feeding protocol and cell types distinguished in the lineage. Confocal
864 Z-projections of the anterior midgut: stained with Hoechst (grey) and showing the cell
865 membrane of ISCs/EBs (magenta, anti-GFP); and showing differentiated ECs (cyan,
866 RFP^+ only) in C and DSS-fed females. Quantification of the percentage of the ISC/EB
867 area (GFP signal) from the total area of the anterior mid gut and of the differentiated
868 ECs (RFP^+ only) from ReDDM cells (RFP^+) in C and DSS-fed females. Although not
869 statistically significant, the increased percentage of ECs in the anterior midgut in DSS-
870 fed animals was a consistent trend in biological replicates of this experiment. C-D)
871 Schematic showing temperature-dependent knock-out of Cdk1 function during the

872 feeding protocol. C) Quantification of PH3/Hoechst positive cells in the anterior midgut
873 and the whole midgut in wild type (heterozygous) and *Cdk1* null females after DSS
874 feeding. D) Quantification of neural tissue in wild-type and *Cdk1* null females after DSS
875 feeding. E) Confocal Z-projections of neuronal processes in the anterior midgut of
876 DSS, DSS + NAC and C +NAC -fed females and quantification of neural tissue. Scale
877 bar 50 μm. Statistical significance is indicated as follows: * $p < 0.05$, ** $p < 0.01$, *** p
878 < 0.001, ns = not significant.
879
880 **Fig. 3. Neural plasticity is not observed in males and masculinization of female**
881 **neurons abolishes neural growth.** A) Confocal Z-projections of neuronal processes
882 in the anterior midgut of C and DSS-fed males, and quantification of neural tissue.
883 Blue outline in box plots indicates male. B-C) Confocal Z-projections at the level of the
884 HCG showing female-specific *tra* alternative splicing in neurons (grey, GFP; magenta,
885 Elav) in females (B) and absence in males (C). D-E) Schematic showing transgene
886 expression in neurons in relation to the feeding protocol. D) Quantification and
887 comparison of neural tissue in females and females with masculinized neurons both
888 in C versus DSS-fed conditions. E) Quantification and comparison of neural tissue in
889 males and males with feminized neurons both in C versus DSS-fed conditions. Scale
890 bar 50 μm. Statistical significance is indicated as follows: * $p < 0.05$, ** $p < 0.01$, *** p
891 < 0.001, ns = not significant.
892
893 **Fig. 4. Neural plasticity in females is required for DSS-induced defecation**
894 **increase and protects against DSS-induced mortality.** A, B) Schematic outlining
895 the timing of defecation assays. Quantification of defecation in a cohort of flies after C
896 or DSS feeding, and after a recovery period: A) on 5% sucrose, or B) on regular food.
897 C) Schematic showing transgene expression and timing of defecation assay.
898 Quantification of defecation after C or DSS feeding in females with wild-type or
899 masculinized neurons. For females with wild-type neurons, controls for the *Gal4/dcr2*
900 and *RNAi/dcr2* transgenes are shown. The three genotypes are color-coded: *Gal4*
901 control in green, *RNAi* control in yellow, and females with masculinized neurons in
902 blue. D) Schematic showing that lifespan analysis covers the 4 days of the feeding
903 assay plus 8 additional of recovery where flies were fed on sucrose. Survival curves
904 of females after C or DSS feeding with wild-type or masculinized neurons, color-coded

as in panel C. When DSS-fed, females with masculinized neurons have a significantly reduced life span compared to females with wild-type neurons (p value=<0,001 for both comparison to *Gal4/dcr2* control and to *RNAi/dcr2* control*)*. For additional comparisons, see Table S2. Statistical significance is indicated as follows: * $p < 0.05$, ** $p < 0.01$, *** $p < 0.001$, ns = not significant.

939 Figure 1

940

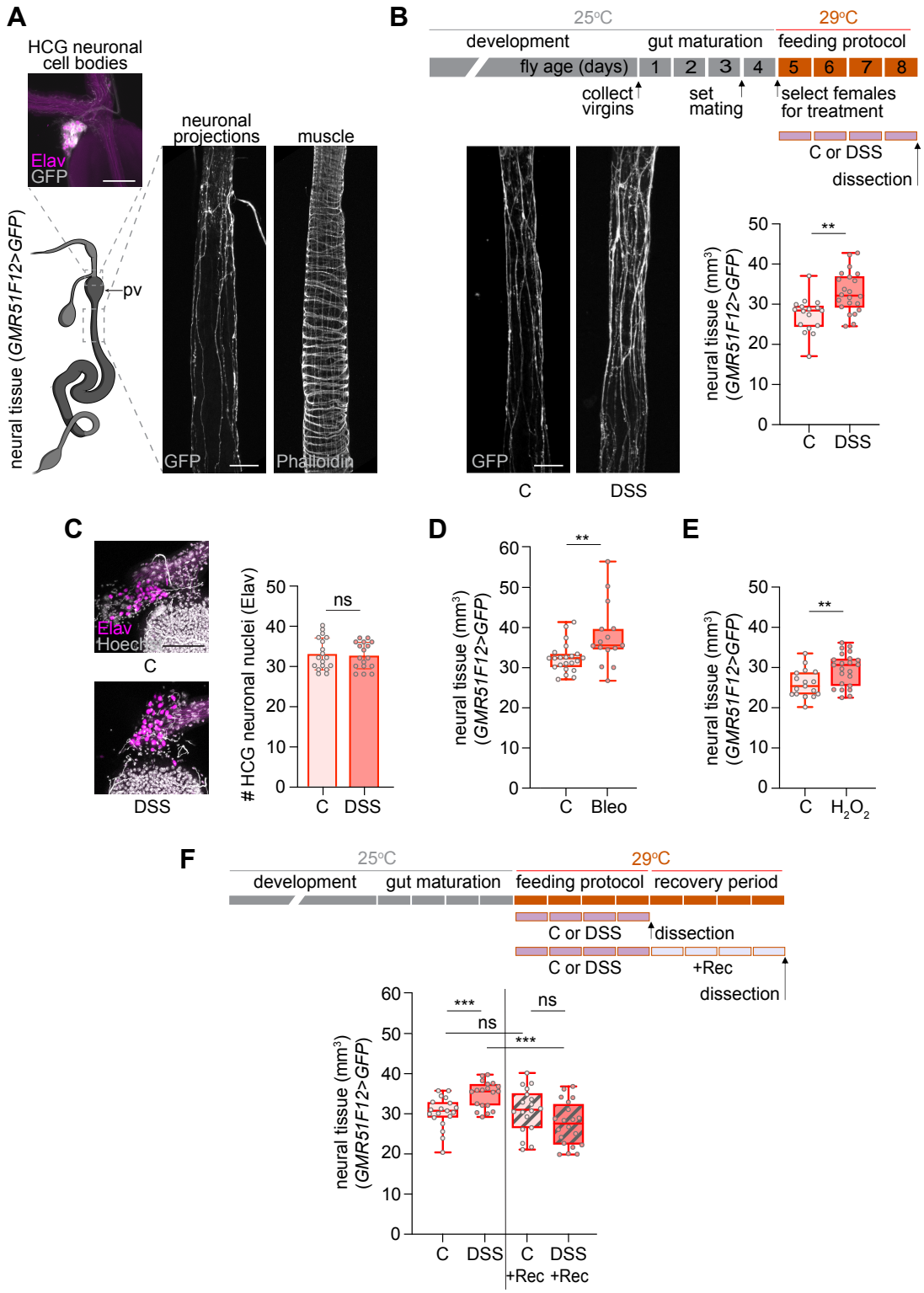

941

942

943

944

945

Figure 2

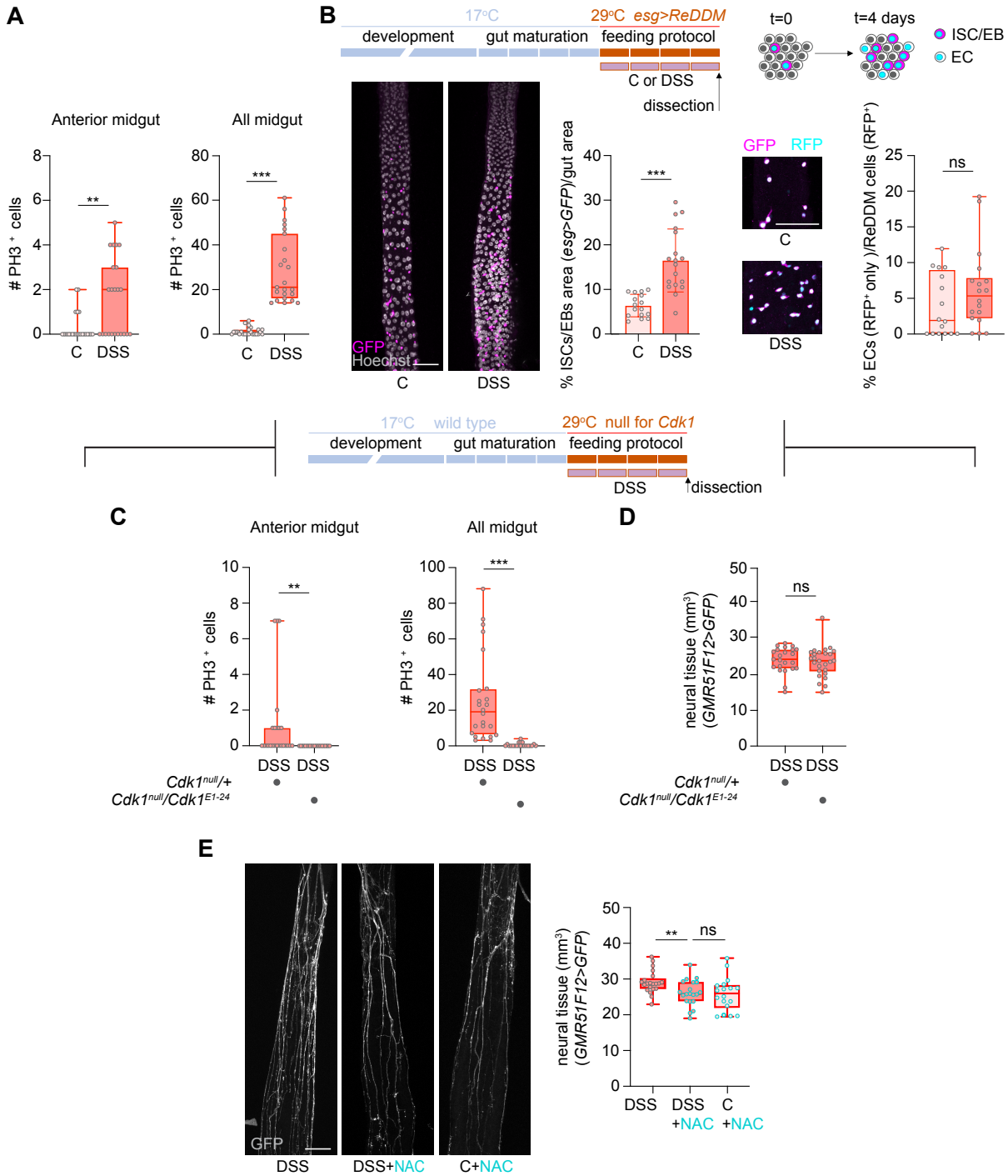
A
Anterior midgut
All midgut
PH3 + cells
C
DSS
B
17°C
29°C esg>ReDDM
development
gut maturation
feeding protocol
C or DSS
dissection
t=0
t=4 days
ISC/EB
EC
GFP
Hoechst
% ISCs/EBs area (esg>GFP)/gut area
GFP RFP
% ECs (RFP+ only)/ReDDM cells (RFP+)
ns
17°C wild type
29°C null for Cdk1
C
D
neural tissue (mm3) (GMR51F12>GFP)
Cdk1null/+
Cdk1null/Cdk1E1-24
E
DSS+NAC
C+NAC
+NAC

Figure 3

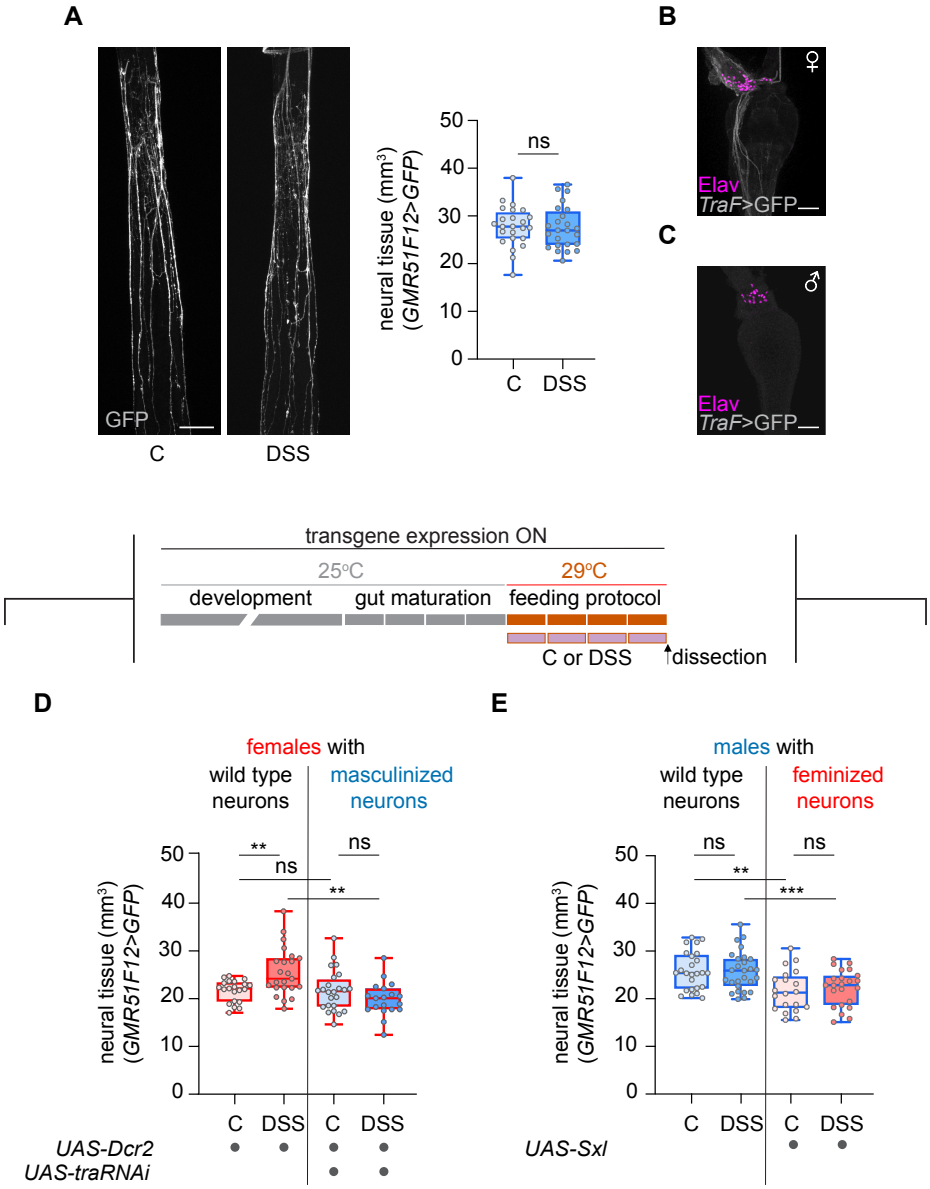
A
GFP
C
DSS
neural tissue (mm³) (GMR51F12>GFP)
ns
C
DSS
B
♀
Elav
TraF>GFP
C
♂
Elav
TraF>GFP
transgene expression ON
25°C
29°C
development
gut maturation
feeding protocol
C or DSS
dissection
D
females with
wild type neurons
masculinized neurons
**
ns
ns
**
UAS-Dcr2
UAS-traRNAi
E
males with
wild type neurons
feminized neurons
ns
**
ns
***
UAS-Sxl

968 Figure 4

969

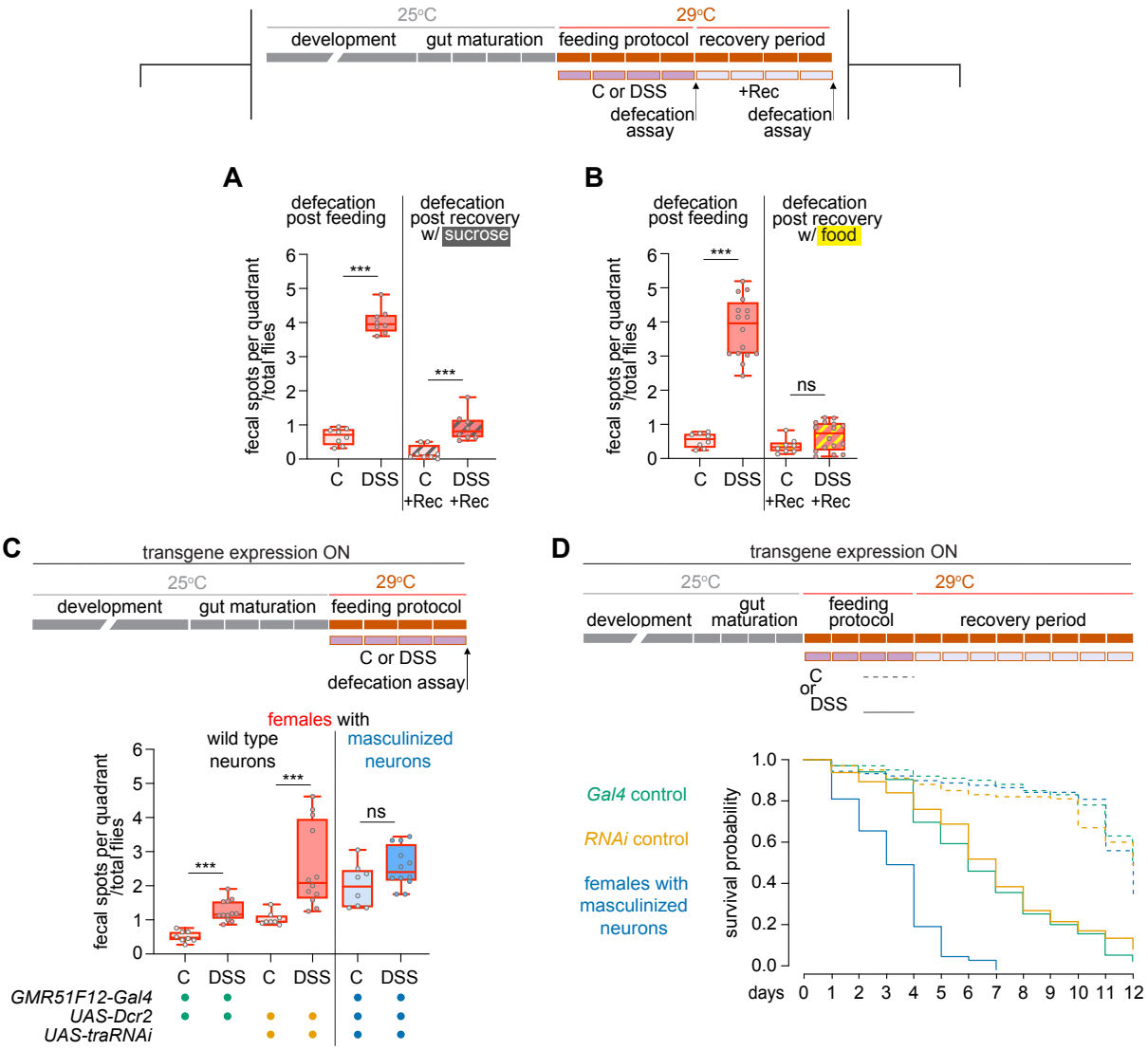

970

971

972

973

974

975

976

977

978

979

980

981